Environmental Science & Technology

ARTICLE

pubs.acs.org/est

Neutron Pair Distribution Function Study of Two-Line Ferrihydrite

Richard Harrington,[*,†,‡] Douglas B. Hausner,[§,⊥] Wenqian Xu,[†] Narayan Bhandari,[§] F. Marc Michel,[¶,#] Gordon E. Brown, Jr.,[¶,#] Daniel R. Strongin,[§] and John B. Parise[†,‡]

[†]Department of Geosciences, Stony Brook University, Stony Brook, New York 11794, United States

[‡]Department of Chemistry, Stony Brook University, Stony Brook, New York 11794, United States

[§]Department of Chemistry, Temple University, Philadelphia, Pennsylvania 19122, United States

[⊥]Department of Chemistry, Rutgers - Camden, Camden, New Jersey 08102, United States

[¶]Department of Geological & Environmental Sciences, Stanford University, Stanford, California 94305, United States

[#]Stanford Synchrotron Radiation Lightsource, SLAC National Accelerator Laboratory, 2575 Sand Hill Road, Menlo Park, California 94025, United States

Supporting Information

ABSTRACT: Pair distribution function (PDF) analysis of neutron total scattering data from deuterated two-line ferrihydrite is consistent with the Keggin-related structural model for ferrihydrite published by Michel et al. (2007). Other models proposed in the literature, such as that of Drits et al. (1993), lead to inferior fits. Bond valence sums indicate that O(1) is bonded to a hydrogen atom, but the quality of the data is such that the exact position of the hydrogen could not be elucidated with confidence.

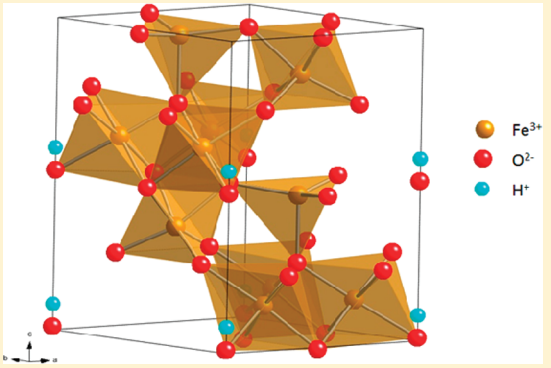

INTRODUCTION

Chemists across a broad range of subdisciplines are interested in the structure of ferrihydrite, an exclusively nanocrystalline iron oxyhydroxide, formed through various synthesis routes.[1] Because of its extremely high surface area and reactivity, industrial chemists utilize ferrihydrite to scavenge heavy metals in the treatment of wastewaters and in processing activities (e.g., direct coal liquefaction and metallurgy[2]). In the environment, ferrihydrite commonly occurs in both pristine (soils and sediments) and contaminated (acid-mine drainage) near-surface environments and acts as an important component in the sequestration and cycling of many transition metals (e.g., chromium[3,4]), nutrient ions (e.g., phosphate[5]), and metalloids (e.g., arsenic[6−9] and antimony[10]) from groundwater, streams, and rivers. Consequently, there has been over 50 years of sustained interest in the structure and properties of this geo-nanomaterial to underpin an understanding of commercial applications, such as engineering of reactive barriers and as a substrate for cleaning up contaminated sites.

Ferrihydrite, also known as hydrous ferric oxide (HFO), was the name given to what was thought to be a range of X-ray amorphous materials. Colloquially, the range of ferrihydrites are represented by the designations 'two-line' and 'six-line' ferrihydrite, so named for the number of broad maxima in the X-ray diffraction patterns collected on laboratory diffractometers. These two 'end-member' ferrihydrites were recently shown to have the same basic atomic arrangement but with different grain sizes; coincidently those sizes are ∼2 nm for two-line and ∼6 nm for six-line ferrihydrite.[11]

Over the past 40+ years, several structural models have been suggested for ferrihydrite.[12−14] A comprehensive review of these early models is given by Jambor and Dutrizac.[1] In 1979, Russell showed by infrared spectroscopy of hydrated and deuterated ferrihydrite that hydrogen is part of the bulk structure, rather than just associated with the surface as water or OH^-.[15]

In 2007, Michel et al.[16] published a structural model for ferrihydrite derived from pair distribution function (PDF) analysis of synchrotron-based X-ray total scattering data. The PDF technique involves taking the Fourier transform of the total scattering structure function, $S(Q)$, which includes both the Bragg and elastic diffuse contributions to the scattering, collected to high wavevector values, Q ($Q = 4\pi \sin\theta/\lambda$).[17] The proposed model derived from the PDF technique is closely related to the Baker−Figgis δ-Keggin cluster and is isostructural with the mineral akdalaite, $Al_{10}O_{14}(OH)_2$, a structure which contains

Received: June 20, 2011
Accepted: September 28, 2011
Revised: September 11, 2011
Published: September 28, 2011

80% octahedral and 20% tetrahedral Al.[18] The presence of tetrahedral iron has been the subject of much controversy over the past several decades.[13,19−22] Manceau et al.,[19] commenting on the structure model put forward by Eggleton and Fitzpatrick,[13] which contained ∼30% tetrahedral Fe, concluded from EXAFS data that there was no four coordinated iron in ferrihydrite. Recently, Maillot et al.,[23] using high resolution EXAFS spectroscopy, have determined the amount of tetrahedral iron in ferrihydrite to be between 20% and 30%, agreeing with the Michel model.

The Michel et al.[16,24] single-phase model has recently been challenged.[25−28] Manceau[26] questioned the single-phase model, preferring instead the three-phase model of Drits et al.[29] The Drits model, based on trial-and-error hand-fitting of laboratory X-ray diffraction data, consists of three distinct phases: a defect-free phase, a defective phase, and an ultradisperse hematite (α-Fe_2O_3) phase. The defect-free phase consists of a hexagonal cell with closest packed oxygens and hydroxyls with iron occupying only octahedral sites, with a 50% probability. The defective phase is more difficult to parametrize, having randomly alternating ABA and ACA stacking. The third phase is ultradisperse hematite, postulated to occur from the inability of the defect-free and defective phase to account for a shoulder in the XRD pattern of at $d = 2.6-2.7$ Å.[29] In a recent paper, Manceau[26] stated that that the third phase may not be exclusively hematite, but could also include maghemite (γ-Fe_2O_3) and magnetite (Fe_3O_4) in proportions which vary from sample to sample. The original Drits et al. paper[29] suggests a 2:1 ratio for the defect-free phase to the defective phase as 2:1 and the ratio of these two phases combined relative to hematite as 3:1.

Two key misconceptions have accompanied criticism of the single-phase model posited by Michel et al.[16] The first[26] involves the nature of scattering from nanocrystals, and the second concerns the use of periodic models to describe the positions of atoms in the limited number of unit cells in a nanocrystal. As to the first misconception,[26] that Bragg scattering calculated from the Michel et al. model does not reproduce the relative intensities of laboratory-derived X-ray diffraction data is hardly surprising.[30−32] It is well-known that diffuse scattering from nanosized grains provides a large contribution to the diffraction pattern and that the relative intensities and *positions* of scattering are influenced by particle size and shape; the diffraction pattern cannot be thought of as simply a series of broadened Bragg peaks.[30,31] One of the rationales for using the Fourier transformed total scattering, i.e., PDF analysis, is that it takes into account the diffuse scattering along with Bragg contributions.[33−37] Furthermore, the distances in the low to intermediate range of the PDF, say less than 15 Å, are less sensitive to the size and shape of nanograins.[38]

Rather than calculating the Bragg scattering alone, Rancourt and Meunier[25] appeared to use the appropriate methodology for calculation of the total scattering in their criticism of the Michel model.[16] Using the Debye equation,[39,40] these authors calculated the X-ray diffraction pattern expected for the Michel et al. model of two-line ferrihydrite for several sizes and shapes of nanoparticles. Despite achieving a reasonable agreement between calculated and experimental data (Figure 3a of Rancourt and Meunier[25]) using trial and error, they dismiss the Michel et al. model as incorrect and do not propose an alternative. It should also be noted that their calculations assumed a population of nanoparticles that is monodisperse and of uniform shape; ferrihydrite, in particular the six-line variety, the focus of that study, is polydisperse and exhibits morphology ranging from subspherical to plate-like.[41] Harrington et al.[38] recently discussed the effect of shape on the diffraction pattern of ferrihydrite and showed that a disk of 2.3 nm by 6 nm fit the X-ray diffraction pattern of six-line ferrihydrite.

The second key misconception concerns the parametrization of the model for atomic arrangements in a nanoparticle. The periodic nature of the Michel model is a necessary idealization. A nanocrystal does possess periodicity, but the periodicity is limited to a small number of unit cells, compared with a traditional single crystal or powder sample. Nonetheless, the concept of the unit cell allows a limited number of parameters to be refined using interatomic distances derived from the PDF. In their original paper,[16] Michel et al. discussed the validity of a periodic model applied to a nanoparticle encompassing very few unit cells. This approach was further discussed by Michel et al.[24] in a study of ferrihydrite aging using time-resolved PDF. They found that two-line ferrihydrite aged in the presence of adsorbed citrate at 175 °C ripened into a ferromagnetic 'ferrifh' phase, which has the same basic structure as two-line ferrihydrite, before transforming to hematite. This intermediate 'ferrifh' phase had more structural relaxation (i.e., less strain and geometrical distortion of polyhedra) and electron spin ordering, leading to the conclusion that this phase has fewer defects than two-line ferrihydrite. From this study, Michel et al. proposed that the stoichiometry of two-line ferrihydrite to be $Fe_{8.2}O_{8.5}(OH)_{7.4}\cdot 3H_2O$. The number of Fe vacancies represented by this formula was estimated based on concurrent changes in total Fe, relative density, and weight losses from thermogravimetric analysis (TGA) as a function of aging.[24] Recently, Xu et al.[42] used TGA and in situ PDF to study the water content of ferrihydrite and changes in the PDF as ferrihydrite transformed directly to hematite to provide constraints on the structure. Note that the ferrimagnetic form of ferrihydrite did not occur as an intermediate phase in the Xu et al.[42] experiments because of intentional differences in experimental conditions. Xu et al. found the OH/Fe ratio to be 0.18, which is slightly less than that predicted by the Michel et al. model (∼0.2) in their 2007 results but much less than that required for the model proposed by Drits et al.[29] or the recently revised Michel et al. model for two-line ferrihydrite that includes a relatively high number of Fe vacancies compensated by structural H (i.e., as OH^-).[24] In addition, Xu et al.[42] used their estimated amount of structural water in two-line ferrihydrite and the interatomic distances observed from PDF analysis of X-ray total scattering data to place constraints on possible anion packing types and local structural motifs in ferrihydrite. The authors demonstrated that ABAC is the only feasible packing type and that the peak at 3.44(2) Å in the PDF provides indirect evidence for the presence of tetrahedral Fe. The results of Xu et al. show good agreement with the original Michel et al. model for ferrihydrite in terms of anion packing sequence, OH/Fe ratio, and the presence of tetrahedral Fe. However, the abundance of Fe vacancies in ferrihydrite and, if vacancies are present, the mechanism of charge-balancing remain unclear and deserve further attention. Developing a better understanding of the position of structural H in ferrihydrite would provide an important new constraint.

With this background, it is clearly advantageous to use neutron diffraction.[43] PDF analysis of neutron total scattering data allows us to test the proposed models for the atomic arrangements in ferrihydrite and compare these results to previous X-ray-based studies. In addition, sensitivity of neutron scattering to light deuterium will allow us to try and elucidate the position and

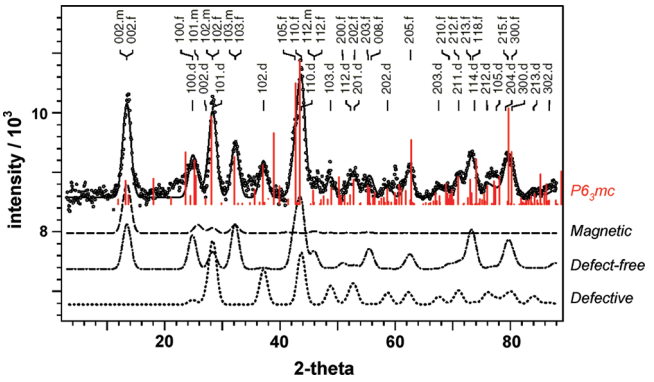

Figure 1. Comparison of the neutron diffraction pattern for a nondeuterated sample of six-line ferrihydrite (dots) to calculated patterns based on the multiphase model (defect-free and defective) originally proposed by Drits et al.[29] The calculated positions and intensities of maxima for the model presented for ferrihydrite by Michel et al.[16] are overlaid (red). Figure reproduced from F. M. Michel's Ph.D. thesis[46] and adapted from that originally presented by Jansen et al.[45]

speciation (i.e., H_2O or OH^-) of H in the bulk structure of ferrihydrite as well as at the surface. Two previous neutron diffraction studies have been performed on ferrihydrite. Seehra et al.[44] compared neutron and X-ray diffraction patterns and determined the peak at $Q = 1.3$ Å^{-1} to be predominantly magnetic. From the temperature dependence of this peak, they concluded that the antiferromagnetic ordering temperature of the core magnetic spins to be $T_N \sim 350$ K. Jansen et al.[45] collected neutron diffraction data on six-line ferrihydrite for structural studies. The samples used were nondeuterated, leading to a high background due to incoherent scattering from hydrogen. In addition, the nanocrystalline nature of the sample led to broadened peaks and a large diffuse scattering contribution, just as in X-ray diffraction studies. Nonetheless, Jansen et al.[45] attempted to fit the defect-free and the defective model to the diffraction data, along with a model for the antiferromagnetic contribution. The overall fit is reasonable, but there was no attempt to fit any of the competing models previously postulated. Michel[46] showed that the single-phase model can also reasonably reproduce these data in terms of peak positions and relative intensities, Figure 1.

With the controversy over the correct structure model for ferrihydrite in mind, we embarked on a program to synthesize highly deuterated two-line ferrihydrite, to study its neutron scattering pattern using PDF methods,[47] and to fit the competing models to these data.

EXPERIMENTAL SECTION

Samples of deuterated two-line ferrihydrite were prepared by modification of the method of Cornell and Schwertmann.[48] All solutions were made with 99.9% D_2O (Cambridge Isotopes) and prepared within a custom-built glovebox purged with dry evaporated nitrogen gas. Solutions of 0.1 M anhydrous ferric chloride (Aldrich) were neutralized using 1 M sodium deuteroxide (Aldrich, 30 wt % in D_2O) solution, resulting in the formation of a suspension of deuterated two-line ferrihydrite. As soon as the pH was stable, samples were centrifuged, dried (rather than dialyzed), washed with D_2O three times, and then dried under a nitrogen atmosphere within the glovebox.

Thermogravimetric analysis (TGA) was carried out under vacuum using a NETZSCH model STA 499 F1 Jupiter simultaneous thermal analyzer by the Thermoanalytical Section of the NETZSCH Instruments Applications Laboratory, Burlington, MA. The sample was heated in an alumina crucible from room temperature to 550 °C at a rate of 10 °C min^{-1}.

Time-of-flight neutron diffraction experiments were carried out on beamline NPDF[49] at the Lujan Center, Los Alamos National Laboratory and the General Materials Diffractometer (GEM) at ISIS,[50] Rutherford Appleton Laboratory, UK. Samples were loaded in a drybox into a vanadium can with an indium-sealed lid to exclude any hydrogen. Samples were run under vacuum and at room temperature. The time required to obtain scattered intensity data with counting statistics suitable for PDF analysis was 8 h.

PDFs were obtained from the measured neutron total scattering by using the software package PDFgetN.[51] Fourier transforms were carried out using a Q_{max} of 35 Å^{-1}. The PDFs were r-averaged over normalization ripples to attempt to smooth the data.[52] The model under investigation was refined using a least-squares 'Rietveld-like' method until the best fit to the data is achieved. This step was performed using the program PDFgui.[53]

Pauling bond valence sums (BVS) were calculated based on the method of Brown and Altermatt[54] around Fe and O atoms using the structural parameters extracted from NPDF analysis. The valence sum V of an atom is the sum of the individual bond valences v_i of the surrounding ligands:

$$V = \sum (v_i)$$

The individual bond valences (v_i) are calculated based on the observed bond length (r):

$$v_i = \exp[(r_0 - r)/B]$$

where r_0 and B are empirically determined values of 1.76 and 0.37, respectively.

RESULTS

Removal of Incoherent Scattering. Because of the large incoherent scattering cross-section of hydrogen, its presence in samples of interest causes a significant increase in the background of a neutron diffraction pattern. The common tactic to mitigate this problem for powdered materials is to deuterate the sample; the two isotopes (^{1}H vs ^{2}D) have different scattering properties, and the incoherent scattering length of D is much smaller than that of H (2.05 vs 80.27 barns, respectively[55]). It is, however, impossible in a practical sense to fully deuterate a sample because of reagent impurity and necessary handling steps, and hence a small amount of H will inevitably be present in a deuterated sample. If the sample is crystalline and a Rietveld refinement is to be performed, the elevated background can be modeled with an empirical function. Indeed, recent studies have shown that, using modern beamlines and software, powder neutron diffraction data for nondeuterated crystalline samples can be successfully refined using Rietveld methods.[56] The task is complicated when performing total scattering studies, as the total Bragg and diffuse component are to be Fourier transformed; it is impossible to differentiate the incoherent scattering from the elastic diffuse scattering. For this reason, it is imperative that the deuteration level is as high as possible.

For nanoparticles, further complications arise from the high surface area. For ferrihydrite, the affinity of the surface for water is high and it is inevitable that a small amount of adventitious water will be in contact with the sample and the H will exchange with

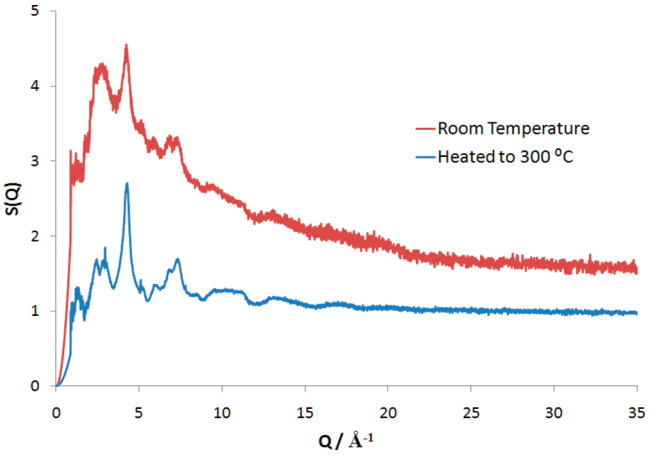

Figure 2. $S(Q)$ vs Q for a sample synthesized and run at room temperature (red) and the same sample after heating in a vacuum at 300 °C for 30 min and then returned to and run at room temperature, avoiding contact with the atmosphere (blue).

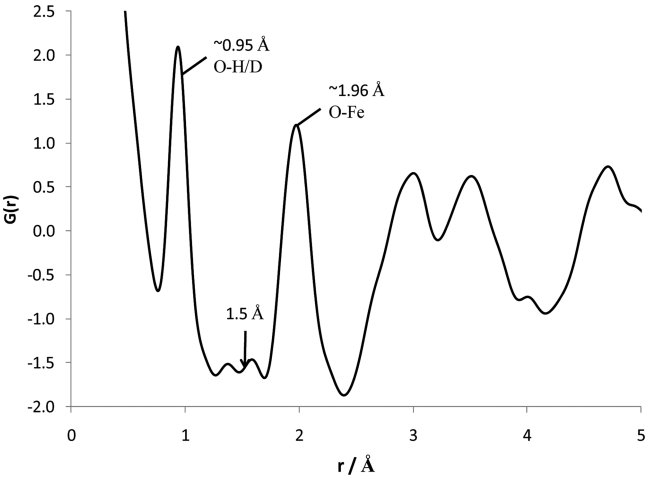

Figure 3. PDF of ferrihydrite run at room temperature prior to heating. The arrow shows the point at r = 1.5 Å, where a H/D-H/D correlation would be if water were present.

the D on the surface. The presence of even a few percent of the ^{1}H isotope is enough to drastically increase background; the incoherent scattering occurs in a random way at all values of Q, although more so at lower Q, and cannot be modeled theoretically. The effect of the incoherent scattering can be seen in the room temperature $S(Q)$ in Figure 2. In an attempt to reduce this background, the final data sets were collected on samples that were heated at 300 °C for 30 min under vacuum and allowed to cool to room temperature before being exposed to the neutron beam. Justification for this heating regime is based on TGA data, Figure S1 (Supporting Information), which shows the loss of most of the surface water without forcing a transformation to hematite. These results are similar to the findings of Xu et al.,[42] who recently also showed that (nondeuterated) ferrihydrite could be heated to ~380 °C for short periods without initiating the transformation to hematite. After this heating regime, much of the background is removed, shown by the blue curve in Figure 2.

Several iron oxide and oxyhydroxide phases were tested against the data to ensure that the chosen heating regime did not bring about the transformation of deuterated ferrihydrite to a more stable phase. Model PDFs calculated from the published structural models of hematite (Fe_2O_3), magnetite (Fe_3O_4), maghemite ($Fe_{2.67}O_4$), lepidocrocite (FeOOH), and goethite (α-FeOOH) were refined individually to the data; none of these models gives a good fit (see Supporting Information). The most likely product of transformation, hematite, clearly does not fit the data, Figure S2 (Supporting Information); the sample is deemed to be ferrihydrite after the heating process.

Surface Species. The PDF of the sample before heating shows a large peak at ~0.95 Å, corresponding to an O−H/D correlation, Figure 3. There is no peak, however, at ~1.5 Å, which would correspond to a D−D correlation in water. This observation suggests that the surface species in ferrihydrite is OH^-, rather than H_2O. As the scattering lengths of H and D are of different signs (−3.7406 and 6.671 fm, respectively[55]), it is possible that a 2:1 ratio of H:D would cause this peak to have zero intensity, although it would also cause the first O−H/D peak to be absent. The peak at 0.95 Å is not observed over the level of the noise in the postheating sample, indicating that the surface OH/D^- has indeed been driven off by the heating regime. Any OD correlations due to the D in the structure are lost in the Fourier ripples at low r.

Structural Model Comparison. A consequence of the ~2−3 nm size of the deuterated ferrihydrite particles is that the number of peaks observed in the PDF is limited with increasing r (Å). It is critical not to overparametrize any of the models tested. By refining a large number of parameters, any model (or mixture of models) can feasibly be fit to such a limited amount of data.

In each of the refinements described below, the instrumental damping factor was set to 0.08 and the spherical particle diameter to 20 Å. As these two parameters are highly correlated and affect data at high r_{ij} more than low r_{ij}, it was decided to set sensible parameters and leave them unrefined.

The Model Proposed by Drits et al.[29] As previously mentioned, the model proposed by Drits et al.[29] consists of three phases: a defective phase, a defect-free phase, and an ultradisperse hematite phase. In the original paper and subsequent publications describing this structure, the exact parametrization is elusive.

As this model consists of three phases, it was decided to refine each phase against the data to see if a reasonable fit could be achieved for any of the proposed phases. The dominant phase is said to be the defect-free phase, which, according to the original 1993 paper, is twice as abundant as the defective phase. The third phase is hematite, which according to Drits et al. is 3 times less abundant than the defective phase. This 6:3:1 defect-free:defective:hematite ratio was constrained in the final refinement. The parameters were taken from the 1993 publication of Drits et al.[29] The overall scale, the lattice parameters, the low r_{ij}-correlated motion[57] parameter (delta), and the z coordinate of the Fe were refined. Isotropic temperature factors were refined but constrained to be equal for each atom of a given type, giving a total of seven refined parameters. Figure S7 (Supporting Information) shows the best fit to the data achieved for the defect-free phase. For this fit, the c lattice parameter changes markedly from the starting values, refining from 9.40 Å to 8.71 Å, a change of 7.3%. The best Rw value achieved for this fit was 50%.

The defective phase is much more difficult to parametrize. Here we use the model proposed in the original 1993 paper,[29]

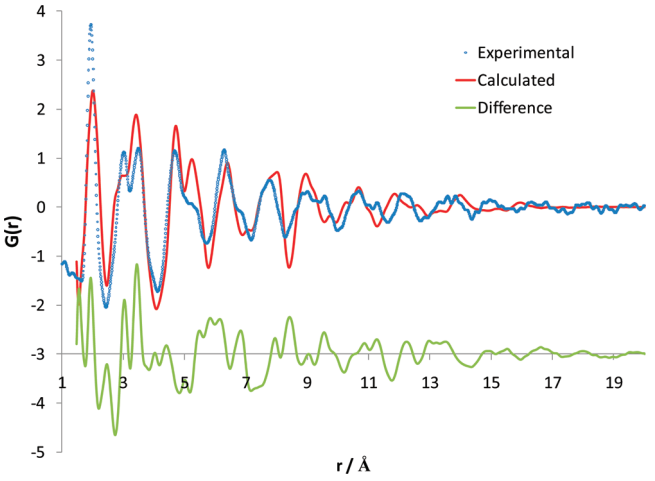

Figure 4. Fit of the Drits model[29] to the neutron data. The blue circles are the experimental data, the red line is the calculated curve, and the green curve is the difference between them. The fit returned an Rw value of 55%.

with *P*3 space group symmetry and lattice parameters a = 2.94 and c = 4.69 Å. This model suggests that there are two iron sites extremely close together, each with 1/4 occupancy; generating a PDF from this model not surprisingly gives rise to two Fe−O correlations, which would give rise to splitting of the first peak. Refinement of the lattice parameters decreases the c parameter until the two Fe sites are equivalent, providing the one Fe−O nearest neighbor pair correlation observed in the data. The third phase in the three-phase model proposed by Drits et al.[29] is ultradisperse hematite. It was shown earlier that hematite provides a poor fit to the experimental PDF, Figure S2.

The simultaneous refinement of the three phases proposed in the original Drits et al.[29] model is shown in Figure 4. A total of 11 parameters were allowed to refine. The problems with the defective phase and hematite are obvious in this fit; the Rw returned was 55%, worse than for the defect-free phase alone, suggesting that the three-phase model is not correct. It may be that our parametrization of the three-phase model is not that intended by its original authors;[29] however, this is a good-faith effort based on the descriptions of the three-phase ferrihydrite model in the literature.

Model Proposed by Michel et al.[16] The starting parameters for the single-phase model are based on the theoretical work by Pinney et al.[58] The model has space group $P6_3mc$, and the atomic coordinates were constrained as such. Scale, lattice parameters, the delta parameter, and isotropic temperature factors were refined. As previously, one temperature factor was refined for each atom type. The starting atomic coordinates were not refined, as the limited amount of data in the PDF cannot support such a high number of variable parameters. A total of seven parameters were allowed to refine in the final fit. At the outset, only the iron and oxygen atoms suggested by Michel et al. were included.

Inclusion of the deuterium atoms in the positions suggested by Pinney et al.,[58] based on the reported structure of the Al analogue, akdalaite,[59] resulted in an increased Rw. Refining the occupancy of the deuterium atoms returned a value of −0.02(22). A second candidate for the position of the deuterium is the 2a site along the c axis, on the opposite side of O1. The position of this deuterium site was calculated assuming an O−H bond length of 0.95 Å. Adding this site improved the goodness of fit by 2%. Applying the Hamilton R-test[60] to this result gives a confidence level of around 60%. Refining the position of the deuterium atoms gives an unrealistically small O−D bond length of 0.65(2) Å. From these results, it is not possible to say definitively the position of the hydrogen atoms. It is also possible that the hydrogen could be disordered between the two sites; the low concentration of structural hydrogen and the noise caused by Fourier ripples at low r make the location of these atoms impossible to determine. An improved data set collected on larger crystals (six-line ferrihydrite) would be required for this more detailed analysis. A full list of parameters is presented in Tables 1 and 2.

Figure 5 shows the final fit to the data for the Michel model. The refined parameters are all close to the starting model, and the global and thermal parameters are reasonable. The reason for the

Table 1. Refined Lattice Parameters, PDF Sharpening, Scale Value, and Residual Factor

a/Å	5.87(2)
c/Å	9.162(66)
δ	0.53(5)
scale/%	0.943(59)
Rw/%	26.9

Table 2. Atomic Coordinates and Isotropic Displacement Parameters

atom	Wyck. pos.	x	y	z	U_{iso}/Å^2
Fe1	6c	0.1668	0.8332	0.6336	
Fe2	2b	1/3	2/3	0.3353	0.0194(26)
Fe3	2b	1/3	2/3	0.9545	
O1	2a	0	0	0.0124	
O2	2b	1/3	2/3	0.7501	0.0106(22)
O3	6c	0.1672	0.8328	0.2368	
O4	6c	0.5145	0.4855	0.0019	

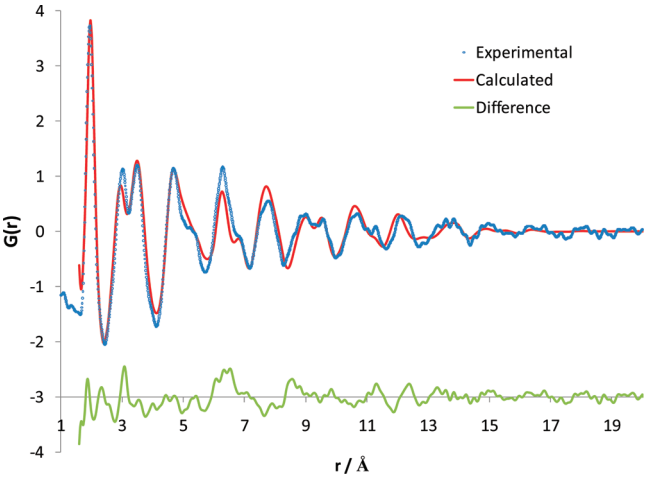

Figure 5. Fit of the Michel model[16] to the neutron data. The blue circles are the experimental data, the red line is the calculated curve, and the green line is the difference between them. The fit returned an Rw value of 26.9%.

Table 3. Bond Valence Sums (Michel et al. model)

	^{VI}Fe1 (6c)			^{VI}Fe2 (2b)			^{IV}Fe3 (2b)					
atom sites	*d* (Å)	mult	BV	*d* (Å)	mult	BV	*d* (Å)	mult	BV	→Σ	total	type
O1 (2a)	2.027	1	0.486							1.46	2.34	OH *
O2 (2b)	2.001	2	0.521				1.873	1	0.737	2.30	2.30	O
O3 (6c)	1.943	2	0.610	1.915	3	0.658				1.88	1.88	O
O4 (6c)	2.024	1	0.490	2.173	3	0.328	1.893	3	0.698	2.01	2.01	O
↓Σ			3.24			2.96			2.83			

less than ideal fit at high *r* is 2-fold. First, the peaks at low *r* are much more intense than those at high *r*, so they have a greater weighting in the least-squares-fitting process. Second, it is at high *r* that grain shape effects are seen in the PDF[31] whereas peaks at low *r* are largely shape independent. PDFgui models the shape using a spherical parameter; as has previously been shown by transmission electron microscopy and recent Debye modeling, the nanoparticles, at least for 6 nm ferrihydrite, are plate-like.[38,48]

The fit quality is also indicated by the calculated BVS for the two octahedral (Fe1 and Fe2) sites and the tetrahedral (Fe3) site that equal 3.19(6), 2.94(6), and 2.82(7) v.u., respectively (Table 3). All three Fe sites are reasonably close to the ideal value of 3 v.u. when considering that ferrihydrite exhibits significant structural disorder. As such, the deviation in calculated BVS for atoms Fe1 and O2 (Table 3) may reflect greater uncertainty in the actual Fe−O bond length obtained from PDF fitting due to local disorder and a distribution of bond lengths. The circumstances appear different in the case of the O1 site where the low BVS of 1.46 v.u. likely indicates that this oxygen is also bonded to H (i.e., hydroxylated). However, adding 0.88 v.u. to account for full hydroxylation of the O1 site results in a total BVS of 2.34 v.u., larger than the ideal value of 2.0 v.u. As in the case of Fe1, the overestimate may reflect uncertainty in terms of the O−Fe bond length. Nevertheless, even partial hydroxylation of the O1 site is consistent with recent findings on the ordered ferrimagnetic form of ferrihydrite.[24]

The recent contribution by Michel et al.[24] states that there are a significant quantity of defects on the octahedral Fe2 and tetrahedral Fe3 site, while the octahedral Fe1 site is fully occupied. They observed that as the particle size increased, the proportion of vacancies decreased. An attempt was made to refine the occupancies of the iron sites to further investigate this. The values returned had a very large error associated with them, indicating the data quality is not sufficient to shed further light on this issue.

We emphasize that the structural model is just that, a model. As with any real sample, some deviation will occur from the model presented. With nanoparticles, these deviations are much more apparent than for more crystalline materials. Vacancies, stacking faults, particle shape, and surface reconstructions (a large percentage of the atoms are at the surface), to name but four, will provide a departure from this idealized model and have effects on the properties, including the scattering of X-rays and neutrons. However, the excellent agreement between the experimental and calculated PDFs suggest that this model is in the large part correct and can be used as a starting point for any further experimental and theoretical studies.

■ ASSOCIATED CONTENT

Ⓢ Supporting Information. TGA data of ferrihydrite under vacuum along with fits to other iron (oxy)hydroxides and to the defect-free and defective phases of the model proposed by Drits. This material is available free of charge via the Internet at http://pubs.acs.org.

■ AUTHOR INFORMATION

Corresponding Author

*Phone: 631-617-1132; e-mail: Richard.Harrington81@gmail.com.

■ ACKNOWLEDGMENT

We acknowledge financial support provided by the National Science Foundation (NSF) through Collaborative Research in Chemistry (CRC), grant number CHE0714183 and CHE0714121. Partial support was also provided by NSF Grant EF-0830093 (Center for Environmental Implications of Nanotechnology) and a DOE-BER SFA grant to the Stanford Synchrotron Radiation Lightsource (FMM and GEB). The authors thank Thomas Proffen, Joan Siewenie, and Katherine Page of Los Alamos National Laboratory for help with data collection and reduction. This work has benefited from the use of the Lujan Center at Los Alamos Neutron Science Center, funded by Department of Energy Office of Basic Energy Sciences and Los Alamos National Laboratory funded by Department of Energy under contract W-7405-ENG-36. We are grateful to Martin Dove, Andrew Goodwin, Dave Keen, and Matt Tucker for help with data collection on GEM. We also thank Nathan Pinney and Dane Morgan of University of Wisconsin, Madison, for help with calculations.

■ REFERENCES

(1) Jambor, J. L.; Dutrizac, J. E. Occurrence and constitution of natural and synthetic ferrihydrite, a widespread iron oxyhydroxide. *Chem. Rev.* **1998**, *98*, 2549–2585.

(2) Huffman, G. P.; Ganguly, B.; Zhao, J.; Rao, K. R. P. M.; Shah, N.; Feng, Z.; Huggins, F. E.; Taghiei, M. M.; Lu, F.; Wender, I.; Pradhan, V. R.; Tierney, J. W.; Seehra, M. S.; Ibrahim, M. M.; Shabtai, J.; Eyring, E. M. Structure and dispersion of iron-based catalysts for direct coal liquefaction. *Energy Fuels* **1993**, *7*, 285–296.

(3) Genc-Fuhrman, H.; Wu, P.; Zhou, Y.; Ledin, A. Removal of As, Cd, Cr, Ni, and Zn from polluted water using an iron based sorbent. *Desalination* **2008**, *226*, 357–370.

(4) Tang, Y.; Michel, F. M.; Zhang, L.; Harrington, R.; Parise, J. B.; Reeder, R. J. Structural properties of the Cr(III)-Fe(III) (oxy)hydroxide compositional series: insights for a nanomaterial "solid solution". *Chem. Mater.* **2010**, *22*, 3589–3598.

(5) Arai, Y.; Sparks, D. L. ATR-FTIR spectroscopic investigation on phosphate adsorption mechanisms at the ferrihydrite-water interface. *J. Colloid Interface Sci.* **2001**, *241* (2), 317–326.

(6) Mohan, D.; Pittman, C. U., Jr. Arsenic removal from water/wastewater using adsorbents - A critical review. *J. Hazard. Mater.* **2007**, *142*, 1–53.

(7) Harrington, R.; Hausner, D. B.; Bhandari, N.; Strongin, D. R.; Chapman, K. W.; Chupas, P. J.; Middlemiss, D. S.; Grey, C. P.; Parise, J. B. Investigations of surface structures by powder diffraction: a differential pair distribution function study on arsenate sorption on ferrihydrite. *Inorg. Chem.* **2010**, *49*, 325–330.

(8) Sherman, D. M.; Randall, S. R. Surface complexation of arsenic(V) to iron(III) (hydr)oxides: Structural mechanism from ab initio molecular geometries and EXAFS spectroscopy. *Geochim. Cosmochim. Acta* **2003**, *67* (22), 4223–4230.

(9) Foster, A. L.; Brown, G. E.; Tingle, T. N.; Parks, G. A. Quantitative arsenic speciation in mine tailings using X-ray absorption spectroscopy. *Am. Mineral.* **1998**, *83* (5−6), 553–568.

(10) Mitsunobu, S.; Teppei, H.; Takahashi, Y. Comparison of antimony behavior with that of arsenic under various soil redox conditions. *Environ. Sci. Technol.* **2006**, *40*, 7270–7276.

(11) Michel, F. M.; Ehm, L.; Liu, G.; Han, W. Q.; Antao, S. M.; Chupas, P. J.; Lee, P. L.; Knorr, K.; Eulert, H.; Kim, J.; Grey, C. P.; Celestian, A. J.; Gillow, J.; Schoonen, M. A. A.; Strongin, D. R.; Parise, J. B. Similarities in 2- and 6-line ferrihydrite based on pair distribution function analysis of X-ray total scattering. *Chem. Mater.* **2007**, *19*, 1489–1496.

(12) Harrison, P. M.; Fischbach, F. A.; Hoy, T. G.; Haggis, G. H. Ferric oxyhydroxide core of ferritin. *Nature* **1967**, *216*, 1188–1190.

(13) Eggleton, R. A.; Fitzpatrick, R. W. New data and a revised structural model for ferrihydrite. *Clays Clay Miner.* **1988**, *36* (2), 111–124.

(14) Towe, K. M.; Bradley, W. F. Mineralogical constitution of colloidal "hydrous ferric oxides. *J. Colloid Interface Sci.* **1967**, *24*, 384–392.

(15) Russell, J. D. Infrared spectroscopy of ferrihydrite: evidence for the presence of structural hydroxyl groups. *Clay Miner.* **1979**, *14*, ;109–114.

(16) Michel, F. M.; Ehm, L.; Antao, S. M.; Lee, P. L.; Chupas, P. J.; Li, G.; Strongin, D. R.; Schoonen, M. A. A.; Phillips, B. L.; Parise, J. B. The structure of ferrihydrite, a nanocrystalline material. *Science* **2007**, *316*, 1726–1729.

(17) Billinge, S. J. L.; Kanatzidis, M. G. Beyond crystallography: the study of disorder, nanocrystallinity and crystallographically challenged materials with pair distribution functions. *Chem. Commun.* **2004**, 749–760.

(18) Yamaguchi, G.; Okumiya, M.; Ono, S. Refinement of the structure of tohdite $5Al_2O_3.H_2O$. *Bull. Chem. Soc. Jpn.* **1969**, *42*, 2247–2249.

(19) Manceau, A.; Combes, J. M.; Calas, G. New Data and a Revised Structural Model for Ferrihydrite - Comment. *Clays Clay Miner.* **1990**, *38* (3), 331–334.

(20) Song, Y.; Bac, B. H.; Lee, Y.-B.; Kim, M. H.; Yoon, W.-S.; Kim, J. H.; Moon, H.-S. Ge-incorporation into six-line ferrihydrite nanocrystals. *CrystEngComm* **2010**, 1997.

(21) Pankhurst, Q. A.; Pollard, R. J. Structural and Magnetic-Properties of Ferrihydrite. *Clays Clay Miner.* **1992**, *40* (3), 268–272.

(22) Carta, D.; Casula, M. F.; Corrias, A.; Falqui, A.; Navarra, G.; Pinna, G. Structural and magnetic characterization of synthetic ferrihydrite nanoparticles. *Mater. Chem. Phys.* **2009**, *113* (1), 349–355.

(23) Maillot, F.; Morin, G.; Wang, Y.; Bonnin, D.; Ildefonse, P.; Chaneac, C.; Calas, G. New insight into the structure of nanocrystalline ferrihydrite: EXAFS evidence for tetrahedrally coordinated iron(III). *Geochim. Cosmochim. Acta* **2011**, *75*, 2708–2720.

(24) Michel, F. M.; Barron, V.; Torrent, J.; Morales, M. P.; Serna, C. J.; Boily, J.-F.; Liu, Q.; Ambrosini, A.; Cismasu, A. C.; Brown, G. E., Jr. Ordered ferrimagnetic form of ferrihydrite reveals links among structure, composition and magnetism. *Proc. Natl. Acad. Sci.* **2010**, *107* (7), 2787–2792.

(25) Rancourt, D. G.; Meunier, J.-F. Constraints on structural models of ferrihydrite as a nanocrystalline material. *Am. Mineral.* **2008**, *93*, 1412–1417.

(26) Manceau, A. Evaluation of the structural model for ferrihydrite derived from real-space modelling of high-energy X-ray diffraction data. *Clay Miner.* **2009**, *44*, 19–34.

(27) Liu, H.; Wang, Y.; Ma, Y.; Wei, Y.; Pan, G. The microstructure of ferrihydrite and its catalytic reactivity. *Chemosphere* **2010**, *79*, 802–806.

(28) Hiemstra, T.; Van Riemsdijk, W. H. A surface structural model for ferrihydrite I: Sites related to primary charge, molar mass, and mass density. *Geochim. Cosmochim. Acta* **2009**, *73*, 4423–4436.

(29) Drits, V. A.; Sakharov, B. A.; Salyn, A. L.; Manceau, A. Structural model for ferrihydrite. *Clay Miner.* **1993**, *28*, 185–207.

(30) Neder, R. B.; Korsunskiy, V. I.; Chory, C.; Muller, G.; Hoffmann, A.; Dembski, S.; Graf, C.; Ruhl, E. Structural characterization of II-VI semiconductor nanoparticles. *Phys. Status Solidi* **2007**, *4* (9), 3123–3396.

(31) Pinna, N. X-ray diffraction from nanocrystals. *Prog. Colloid Polym. Sci.* **2005**, *130*, 29–32.

(32) Hall, B. D. Debye function analysis of structure in diffraction from nanometer-sized particles. *J. Appl. Phys.* **2000**, *87* (4), 1666–1675.

(33) Neder, R. B.; Korsunskiy, V. I. Structure of nanoparticles from powder diffraction data using the pair distribution function. *J. Phys.: Condens. Matter* **2005**, *17*, S125–S134.

(34) Korsunskiy, V. I.; Neder, R. B.; Hoffmann, A.; Dembski, S.; Graf, C.; Ruhl, E. Aspects of the modelling of the radial distribution function for small nanoparticles. *J. Appl. Crystallogr.* **2007**, *40*, 975–985.

(35) Korsunskiy, V. I.; Neder, R. B. Exact model calculations of the total radial distribution functions for the x-ray diffraction case and systems of complicated chemical compositions. *J. Appl. Crystallogr.* **2005**, *38*, 1020–1027.

(36) Billinge, S. J. L. Local structure from total scattering and atomic pair distribution function (PDF) analysis. In *Powder Diffraction: Theory and Practice*; Dinnebier, R. E.; Billinge, S. J. L., Eds.; Royal Society of Chemistry, London, England, 2008.

(37) Proffen, T.; Page, K. L. Obtaining structural information from the atomic pair distribution function. *Z. Kristallogr.* **2004**, *219*, 130–135.

(38) Harrington, R.; Neder, R. B.; Parise, J. B. The nature of x-ray scattering from geo-nanoparticles: practical considerations of the use of the Debye equation and the pair distribution function for structure analysis. *Chem. Geol.* **2011**, doi: 10.1016/j.chemgeol.2011.06.010.

(39) Debye, P. Dispersion of Roentgen rays. *Ann. Phys.* **1915**, *46*, 809.

(40) Warren, B. E. *X-ray diffraction*; Dover: New York, 1990.

(41) Janney, D. E.; Cowley, J. M.; Buseck, P. R. Transmission electron microscopy of synthetic 2-and six-line ferrihydrite. *Clays Clay Miner.* **2000**, *48* (1), 111–119.

(42) Xu, W.; Hausner, D. B.; Harrington, R.; Lee, P. L.; Strongin, D. R.; Parise, J. B. Structural water in ferrihydrite and constraints this provides on possible structure models. *Am. Mineral.* **2011**, *96* (4), 513–520.

(43) Dove, M. T. An introduction to the use of neutron scattering methods in mineral sciences. *Eur. J. Miner.* **2002**, *14*, 203–224.

(44) Seehra, M. S.; Babu, V. S.; Manivannan, A.; Lynn, J. W. Neutron scattering and magnetic studies of ferrihydrite nanoparticles. *Phys. Rev. B* **2000**, *61* (5), 3513–3518.

(45) Jansen, E.; Kyek, A.; Schafer, W.; Schwertmann, U. The structure of six-line ferrihydrite. *Appl. Phys. A: Mater. Sci. Process.* **2002**, *74* (Suppl.), S1004–S1006.

(46) Michel, F. M. Structure determination of nanocrystalline materials. Ph.D. Thesis, Stony Brook University, 2007.

(47) Qiu, X.; Bozin, E. S.; Juhas, P.; Proffen, T.; Billinge, S. J. L. Recirocal-space instrumental effects on the real-space neutron atomic pair distribution function. *J. Appl. Crystallogr.* **2004**, *37*, 110–116.

(48) Schwertmann, U.; Cornell, R. M. *Iron oxides in the laboratory*; Wiley-VCH: New York, 1991; p 188.

(49) Proffen, T.; Egami, T.; Billinge, S. J. L.; Cheetham, A. K.; Louca, D.; Parise, J. B. Building a high resolution total scattering powder diffractometer - upgrade of NPD at MLNSC. *Appl. Phys. A: Mater. Sci. Process.* **2002**, *74*, S163–S165.

(50) Williams, W. G.; Ibberson, R. M.; Day, P.; Enderby, J. E. GEM - General materials diffractometer at ISIS. *Phys. B* **1998**, *241−243* (234−236), 234.

(51) Peterson, P. F.; Gutmann, M.; Proffen, T.; Billinge, S. J. L. PDFgetN: a user friendly program to extract the total scattering structure factor and the pair distribution function from neutron powder diffraction data. *J. Appl. Crystallogr.* **2000**, *33*, 1192.

(52) Chapman, K. W.; Chupas, P. J.; Maxey, E. R.; Richardson, J. W. Direct observtion of adsorbed H_2-framework interactions in the

Prussian Blue analogue $Mn^{II3}[Co^{III}(CN)_6]_2$: The relative importance of accessible coordination sites and van der Waals interactions. *Chem. Commun.* **2006**, *38*, 4013–4015.

(53) Farrow, C. L.; Juhas, P.; Liu, J. W.; Bryndin, D.; Bozin, E. S.; Bloch, J.; Proffen, T.; Billinge, S. J. L. PFDfit2 and PDFgui: computer programs for studying nanostructures in crystals. *J. Phys.: Condens. Matter* **2007**, *19*, 335219.

(54) Brown, I. D.; Altermatt, D. Bond-Valence Parameters Obtained from a Systematic Analysis of the Inorganic Crystal-Structure Database. *Acta Crystallogr., Sect. B: Struct. Sci.* **1985**, *41* (Aug), 244–247.

(55) Sears, V. F. Neutron scattering lengths and cross sections. *Neutron News* **1992**, *3* (3), 26–37.

(56) Weller, M. T.; Henry, P. F.; Ting, V. P.; Wilson, C. C. Crystallography of hydrogen-containing compounds: realizing the potential of neutron powder diffraction. *Chem. Commun.* **2009**, 2973–2989.

(57) Jeong, I.-K.; Proffen, T.; Mohiuddin-Jacobs, F.; Billinge, S. J. L. Measuring correlated motion using X-ray diffraction. *J. Phys. Chem. A* **1999**, *103* (7), 921–924.

(58) Pinney, N.; Kubicki, J. D.; Middlemiss, D. S.; Grey, C. P.; Morgan, D. Density functional theory study of ferrihydrite and related Fe-oxyhydroxides. *Chem. Mater.* **2009**, *21*, 5727–5742.

(59) Demichelis, R.; Noel, Y.; Zicovich-Wilson, C. M.; Roetti, C.; Valenzano, L.; Dovesi, R. *Ab-initio* quantum mechanical study of akdalaite ($5Al_2O_3.H_2O$): structure and vibrational spectrum. *J. Phys.: Conf. Ser.* **2008**, *117*, 012013.

(60) Hamilton, W. C. Significance Tests on Crystallographic R Factor. *Acta Crystallogr.* **1965**, *18*, 502–510.